 CMES, vol.90, no.4, pp.283-301, 2013

Analysis of Band Structure for 2D Acoustic Phononic Structure by BEM and the Block SS Method

H.F. Gao[1], T. Matsumoto[1], T. Takahashi[1] and H. Isakari[1]

Abstract: By its very basis, the block Sakurai-Sugiura (SS) method may be applied to solving nonlinear eigenvalue problem formulated by boundary integral equation. In this paper, the methodology of BEM combined with the block SS method is applied to the computation of band structures of phononic structures for acoustic problems. Since the conventional boundary integral equation yields the real fictitious eigenfrequencies when it is applied to an exterior problem of scatters, Burton-Miller's method is employed to remove the real fictitious eigenfrequencies resulted by the boundary of the scatterers. The application of the method is demonstrated through analyses of band structures of homogenous and composite structures.

Keywords: phononic structure, band structure, block Sakurai-Sugiura method, BEM, eigenfrequencies.

1 Introduction

The composite structures so-called phononic crystals, which show band structures for acoustic/elastic waves, are considered as elastic analogous extensions of photonic crystals. The existence of bandgaps in phononic crystals is also observed by both theoretical studies [Kushwaha, Halevi, Dobrzynski, and Djafari-Rouhani (1993); Sigalas and Economou (1993)] and experimental investigations [Parmley, Zobrist, Clough, Perez-Miller, Makela, and Yu (1995); Martínez-Sala, Sancho, Sánchez, Gómez, and Llinares (1995)]. It is shown that the propagation of elastic waves with particular frequencies within bandgaps is forbidden by the phononic crystals. This property enables phononic crystals to provide a sound and vibration isolated environment as a result of the created bandgaps. Furthermore, phononic crystals can also be used as wave filters or waveguides with a moderate number of dot defects or linear defects distributed in a certain way [Sigalas (1998); Khelif,

[1] Department of Mechanical Science and Engineering, Nagoya University, Nagoya, Aichi, Japan.

Djafari-Rouhani, Vasseur, and Deymier (2003); Khelif, Choujaa, Djafari-Rouhani, Wilm, Ballandras, and Laude (2003)].

Several numerical methods have already been developed for computation of band structures of phononic crystals, for example, plane wave expansion (PWE) method [Kushwaha, Halevi, Dobrzynski, and Djafari-Rouhani (1993); Sigalas and Economou (1993); Goffaux and Vigneron (2001)], multiple-scattering theory (MST) method [Kafesaki and Economou (1999); Psarobas, Stefanou, and Modinos (2000); Liu, Chan, and Sheng (2002)], finite difference time domain (FDTD) method [Tanaka, Tomoyasu, and Tamura (2000); Vasseur, Deymier, Khelif, Lambin, Djafari-Rouhani, Akjouj, Dobrzynski, Fettouhi, and Zemmouri (2002); Wang, Wen, Han, and Zhao (2003)], wavelet method [Yan and Wang (2006)] and finite element method (FEM).

The research interest in the analysis of phononic crystals is the bandgaps searching. Similar to photonic crystals, numerical analyses of bandgaps for phononic crystals usually result in eigenvalue problems. The boundary element method (BEM) is one of the widely used numerical computation tools for wave problems, requiring the discretization of the boundary only. For scattering problems, it satisfies the radiation conditions by giving appropriate Green's function. There are two methodologies of analysis for periodic composite structures: one is to give the Bloch conditions on a unit cell and use the conventional Green's function [Li, Wang, and Zhang (2012)], and the other is to apply the Bloch conditions directly to the wave equation [Knipp and Reinecke (1998); Barnett and Greengard (2010)]. However, both methodologies result in nonlinear eigenvalue problems when they are applied to obtaining dispersion curves of phononic crystals. The transcendental eigen equation makes it difficult to solve the eigenvalues by standard eigensolvers directly. For photonic crystals, there is a work in which the nonlinear eigenvalue problem is converted to a generalized one by transforming the system matrix with the former methodology [Li, Wang, and Zhang (2012)].

The Sakurai-Sugiura (SS) Method [Sakurai and Sugiura (2003); Asakura, Sakurai, Tadano, Ikegami, and Kimura (2003); Ikegami, Sakurai, and Nagashima (2010)], is a numerical technique for solution of eigenvalue problems. It has been applied to generalized and nonlinear eigenvalue problems. It is claimed that the SS method has the capability of reducing the eigenspace of the original nonlinear eigenvalue problems and extracting the desired eigenvalues located within a certain domain of complex plane. The SS method has been applied to calculations of core-excited states of formaldehyde [Tsuchimochi, Kobayashi, Nakata, Imamura, and Nakai (2008)] and resonance of 2D acoustic cavity combined with BEM [Gao, Matsumoto, Takahaishi, and Yamada (2011)], and its capability of parallel calculation [Sakurai, Kodaki, Tadano, Takahashi, Sato, and Nagashima (2008)] may make the

equations formulated by BEM easy to be solved on different processors independently.

The present work offers a methodology of band structrure calculation for two-dimensional phononic crystals. BEM combined with the block SS method is employed to compute dispersion curves. The constant elements are adopted for simplicity of numerical treatment. We have to mention that the scattering problem analyzed by BEM yields fictitious frequencies, which can be removed by Burton-Miller's method [Burton and Miller (1971)]. The application of the technique is demonstrated through bandgap analyses of homogenous and composite structures. The results show the effectiveness of the proposed method.

2 Formulation

2.1 Governing equation

The propagation of time-harmonic acoustic waves in a homogeneous and isotropic medium is governed by Helmholtz's equation:

$$\nabla^2 p(\mathbf{x}) + k^2 p(\mathbf{x}) = 0 \quad \text{in } D, \tag{1}$$

where $p(\mathbf{x})$ is the sound pressure at a point $\mathbf{x}$ in the domain D, ∇^2 is Laplace's operator, $k = \frac{\omega}{c}$ is the wave number, ω is the circular frequency, c is the wave speed.

The boundary condition on the boundary S is given as

$$p(\mathbf{x}) = \bar{p}(\mathbf{x}) \quad \text{on } S_p, \tag{2}$$

$$q(\mathbf{x}) = \frac{\partial p}{\partial n}(\mathbf{x}) = \mathrm{i}\rho\omega\bar{v}(\mathbf{x}) \quad \text{on } S_q, \tag{3}$$

$$p(\mathbf{x}) = \mathrm{z}v(\mathbf{x}) \quad \text{on } S_\mathrm{z}, \tag{4}$$

where $n(\mathbf{x})$ is outward normal to the boundary S at point $\mathbf{x}$, i is the imaginary unit, ρ is the density of the medium, v is the particle velocity in the outward normal direction, and z is the acoustic impedance.

Since no energy is radiated from the infinity to the field, the sound pressure p must satisfy the Sommerfeld radiation condition:

$$\lim_{|\mathbf{x}|\to+\infty} |\mathbf{x}|^{\frac{\tau-1}{2}} \left(\frac{\partial p(\mathbf{x})}{\partial |\mathbf{x}|} - \mathrm{i}kp(\mathbf{x}) \right) = 0, \tag{5}$$

where τ=2 for 2D case.

2.2 Boundary integral equations

The integral representation for Eq. (1) is written as

$$p(\mathbf{x}) + \int_S q^*(\mathbf{x},\mathbf{y}) p(\mathbf{y}) \mathrm{d}S(\mathbf{y}) - \int_S p^*(\mathbf{x},\mathbf{y}) q(\mathbf{y}) \mathrm{d}S(\mathbf{y}) = 0, \quad \mathbf{x} \text{ in } D, \tag{6}$$

where p^* is the fundamental solution of Helmholtz's equation in 2D, given as

$$p^*(\mathbf{x},\mathbf{y}) = \frac{\mathrm{i}}{4} H_0^{(1)}(kr), \tag{7}$$

$$q^*(\mathbf{x},\mathbf{y}) = \frac{\partial p^*(\mathbf{x},\mathbf{y})}{\partial n(\mathbf{y})} = -\frac{k\mathrm{i}}{4} H_1^{(1)}(kr) \frac{\partial r}{\partial n(\mathbf{y})}, \tag{8}$$

where $r = |\mathbf{x} - \mathbf{y}|$, $\mathbf{x}$ and $\mathbf{y}$ are two different points, $n(\mathbf{y})$ is the normal direction on the boundary at the point $\mathbf{y}$, $H_0^{(1)}$ and $H_1^{(1)}$ are the Hankel functions of the first kind of zero and first order, respectively.

The normal derivative of Eq. (6) at the point x is written as

$$q(\mathbf{x}) + \int_S \hat{q}^*(\mathbf{x},\mathbf{y}) p(\mathbf{y}) \mathrm{d}S(\mathbf{y}) - \int_S \hat{p}^*(\mathbf{x},\mathbf{y}) q(\mathbf{y}) \mathrm{d}S(\mathbf{y}) = 0 \quad \text{in } D, \tag{9}$$

where $\hat{p}^*(\mathbf{x},\mathbf{y})$ and $\hat{q}^*(\mathbf{x},\mathbf{y})$ are the normal derivatives of $p^*(\mathbf{x},\mathbf{y})$ and $q^*(\mathbf{x},\mathbf{y})$ at point $\mathbf{x}$, respectively, as follows:

$$\hat{p}^*(\mathbf{x},\mathbf{y}) = \frac{\partial p^*(\mathbf{x},\mathbf{y})}{\partial n(\mathbf{x})} = -\frac{k\mathrm{i}}{4} H_1^{(1)}(kr) \frac{\partial r}{\partial n(\mathbf{x})}, \tag{10}$$

$$\begin{aligned} \hat{q}^*(\mathbf{x},\mathbf{y}) &= \frac{\partial q^*(\mathbf{x},\mathbf{y})}{\partial n(\mathbf{x})} \\ &= -\frac{k^2\mathrm{i}}{8} [H_0^{(1)}(kr) - H_2^{(1)}(kr)] \frac{\partial r}{\partial n(\mathbf{x})} \frac{\partial r}{\partial n(\mathbf{y})} \\ &\quad -\frac{k\mathrm{i}}{4} H_1^{(1)}(kr) \frac{\partial^2 r}{\partial n(\mathbf{x}) \partial n(\mathbf{y})}. \end{aligned} \tag{11}$$

Let x approach the boundary S, then the conventional boundary integral equation (CBIE) can be obtained from Eq. (6), as

$$C(\mathbf{x}) p(\mathbf{x}) + \fint_S q^*(\mathbf{x},\mathbf{y}) p(\mathbf{y}) \mathrm{d}S(\mathbf{y}) - \int_S p^*(\mathbf{x},\mathbf{y}) q(\mathbf{y}) \mathrm{d}S(\mathbf{y}) = 0. \tag{12}$$

where $\fint$ denotes that the integral is evaluated in the sense of Cauchy-principal value (CPV), $C(\mathbf{x})$ depends on the geometry of boundary S at point $\mathbf{x}$, and for smooth boundary $C(\mathbf{x}) = 1/2$.

Similarly, from Eq. (9), the normal derivative boundary integral equation (NDBIE) is obtained as

$$C(\mathbf{x})q(\mathbf{x}) + \oint\!\!\!\!\!\!= \int_S \hat{q}^*(\mathbf{x},\mathbf{y})p(\mathbf{y})\mathrm{d}S(\mathbf{y}) - \int_S \hat{p}^*(\mathbf{x},\mathbf{y})q(\mathbf{y})\mathrm{d}S(\mathbf{y}) = 0, \tag{13}$$

where $\oint\!\!\!\!\!\!=$ denotes that the integral is evaluated in the sense of finite-part of divergent integral [Zheng, Chen, Matsumoto, and Takahashi (2011)]. We can also eliminate the hyper-singularity in Eq. (13) using regularization method [Qian, Han, Ufimtsev, and Atluri (2004); Qian, Han, and Atluri (2004)].

Combining the CBIE and NDBIE, we can write the integral equation for Burton-Millier's method as follows,

$$\begin{aligned}&\frac{1}{2}p(\mathbf{x}) + \oint\!\!\!\!\!\!= q^*(\mathbf{x},\mathbf{y})p(\mathbf{y})\mathrm{d}S(\mathbf{y}) - \int_S p^*(\mathbf{x},\mathbf{y})q(\mathbf{y})\mathrm{d}S(\mathbf{y})\\ &+\frac{1}{2}\alpha q(\mathbf{x}) + \alpha\oint\!\!\!\!\!\!= \hat{q}^*(\mathbf{x},\mathbf{y})p(\mathbf{y})\mathrm{d}S(\mathbf{y}) - \alpha\int_S \hat{p}^*(\mathbf{x},\mathbf{y})q(\mathbf{y})\mathrm{d}S(\mathbf{y}) = 0,\end{aligned} \tag{14}$$

where α is the coefficient of Burton-Miller's method. In this study, α is chosen as $\mathrm{i}/2k$.

Discretizing Eq. (14) with n constant elements, the discretized form of the boundary integral equation is obtained, as follows:

$$\begin{aligned}&\frac{1}{2}p^i(\mathbf{x}) + \frac{1}{2}\alpha q^i(\mathbf{x}) + \sum_{j=1}^{n}\int_{S_j}\left[q^*(\mathbf{x},\mathbf{y}) + \alpha\hat{q}^*(\mathbf{x},\mathbf{y})\right]\mathrm{d}S(\mathbf{y})p^j(\mathbf{y})\\ &-\sum_{i=1}^{n}\int_{S_j}\left[p^*(\mathbf{x},\mathbf{y}) + \alpha\hat{p}^*(\mathbf{x},\mathbf{y})\right]\mathrm{d}S(\mathbf{y})q^j(\mathbf{y}) = 0,\end{aligned} \tag{15}$$

where S_j denotes the j-th element, p^j, q^j are the sound pressure and its normal derivative on the S_j element respectively. Let the integrals in Eq. (15) be denoted as

$$\hat{B}^{ij} = \int_{S_j}\left[q^*(\mathbf{x},\mathbf{y}) + \alpha\hat{q}^*(\mathbf{x},\mathbf{y})\right]\mathrm{d}S(\mathbf{y}), \tag{16}$$

$$\hat{G}^{ij} = \int_{S_j}\left[p^*(\mathbf{x},\mathbf{y}) + \alpha\hat{p}^*(\mathbf{x},\mathbf{y})\right]\mathrm{d}S(\mathbf{y}). \tag{17}$$

Furthermore, let us write

$$B^{ij} = \begin{cases}\hat{B}^{ij} & i \neq j\\ \hat{B}^{ij} + \frac{1}{2} & i = j\end{cases}, \tag{18}$$

and

$$G^{ij} = \begin{cases} \hat{G}^{ij} & i \neq j \\ \hat{G}^{ij} + \frac{1}{2} & i = j \end{cases} . \tag{19}$$

By using the representations in Eqs. (18) and (19), Eq. (15) is written as

$$\sum_{j=1}^{n} B^{ij} p^j = \sum_{j=1}^{n} G^{ij} q^j. \tag{20}$$

Assuming the fundamental solution is applied at each center of the constant element, a system of algebraic equations is obtain in the matrix form:

$$\begin{pmatrix} B^{11} & B^{12} & \cdots & B^{1n} \\ B^{21} & B^{22} & \cdots & B^{2n} \\ \vdots & \vdots & \ddots & \vdots \\ B^{n1} & B^{n2} & \cdots & B^{nn} \end{pmatrix} \begin{pmatrix} p^1 \\ p^2 \\ \vdots \\ p^n \end{pmatrix} = \begin{pmatrix} G^{11} & G^{12} & \cdots & G^{1n} \\ G^{21} & G^{22} & \cdots & G^{2n} \\ \vdots & \vdots & \ddots & \vdots \\ G^{n1} & G^{n2} & \cdots & G^{nn} \end{pmatrix} \begin{pmatrix} q^1 \\ q^2 \\ \vdots \\ q^n \end{pmatrix}, \tag{21}$$

or

$$\mathbf{Bp} = \mathbf{Gq}, \tag{22}$$

where $\mathbf{B}$ and $\mathbf{G}$ are $n \times n$ matrices, $\mathbf{p}$ and $\mathbf{q}$ are vectors that contain the sound pressure and its normal derivative of the boundary element, respectively. Moreover, in this work, both vectors are unknowns but have certain periodic relations given by extra equations, which are discussed in the following section.

2.3 Periodic boundary conditions and the eigenvalue problem

Let us consider a 2D phononic structure as shown in Fig. 1. The cylindrical scatterers, infinitely long in z direction, are periodically collocated in the matrix medium that is assumed to be air in this study. With the radius of the cylinders R, and the lattice constant a, the filling fraction can be obtained as follows,

$$f = \pi R^2 / a^2. \tag{23}$$

To calculate the band structure, we need to analyze only a unit cell shown in Fig. 2(a), and apply the periodic boundary condition on the boundary of the unit cell. The reciprocal lattice and the first Brillouin zone are shown in Fig. 2(b). $\mathbf{k} = (k_x, k_y)$ is the Bloch wavevector in x-y plane.

The periodic structure requires that the sound pressure $p(\mathbf{x})$ must satisfy the following relationship according to the Bloch theorem:

$$p(\mathbf{x} + \mathbf{l}) = \mathrm{e}^{\mathrm{i}\mathbf{k}\cdot\mathbf{l}} p(\mathbf{x}), \tag{24}$$

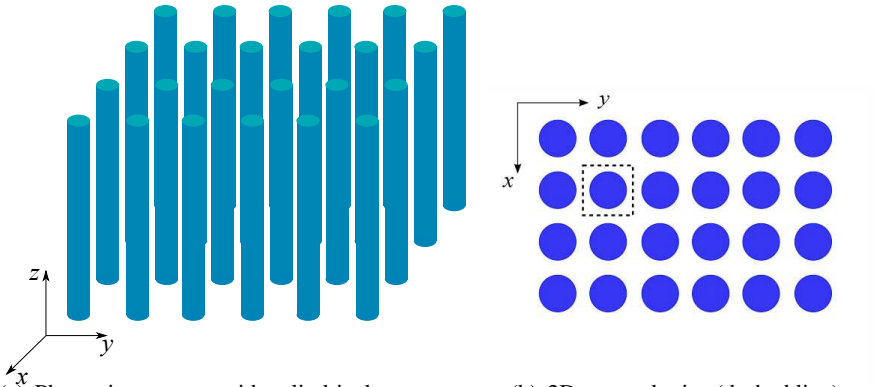

(a) Phononic structure with cylindrical scatterers. (b) 2D square lattice (dashed line).

Figure 1: 2D Phononic crystal.

where $\mathbf{l} = n_1\mathbf{a}_x + n_2\mathbf{a}_y$ is the translation vector, $\mathbf{a}_x$, $\mathbf{a}_y$ are the lattice base vectors. The periodic boundary condition is applied on the boundary elements of the unit cell, which restricts the infinite problem to a bounded one. Because of the symmetry of the Brillouin zone, we let the wave vector vary only along the boundary of the first Brillouin zone: $\mathrm{M} \to \Gamma \to \mathrm{X} \to \mathrm{M}$. Then, all the waves propagating in the composite structure are obtained.

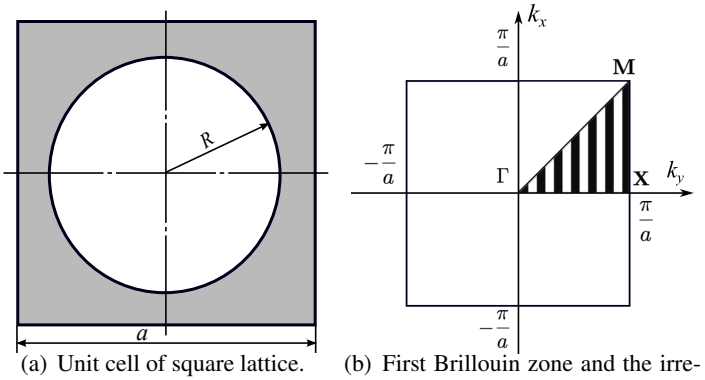

(a) Unit cell of square lattice. (b) First Brillouin zone and the irreducible Brillouin zone (shade).

Figure 2: Unit cell and Brillouin zone.

In order to introduce the periodic boundary condition, we separate the elements into three groups: (i) the dependent elements; (ii) the independent elements; (iii) the internal elements, which are illustrated in Fig. 3. The dependent elements

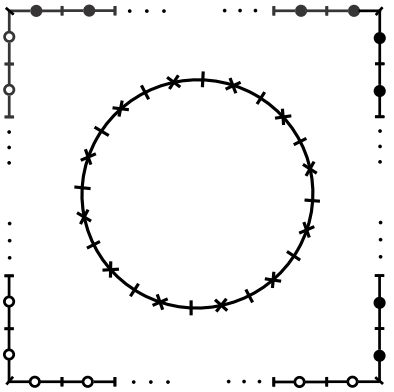

Figure 3: The meshed model of the unit cell. The open circular symbols denote the independent element; the solid circular symbols denote the dependent element; the cross symbols denote the internal elements

are represented by open circular symbols, the independent elements are by solid circular ones, and internal elements are by cross symbols.

We define the quantities corresponding to the three element groups represented by the following expressions:

$\mathbf{p}^D, \mathbf{q}^D$: Nodal sound pressure and normal derivative at dependent elements.

$\mathbf{p}^I, \mathbf{q}^I$: Nodal sound pressure and normal derivative at independent elements.

$\mathbf{p}^C, \mathbf{q}^C$: Nodal sound pressure and normal derivative at internal elements.

With the above definitions, Eq. (22) can be written as

$$\begin{pmatrix} \mathbf{B}^D & \mathbf{B}^I & \mathbf{B}^C \end{pmatrix} \begin{pmatrix} \mathbf{p}^D \\ \mathbf{p}^I \\ \mathbf{p}^C \end{pmatrix} = \begin{pmatrix} \mathbf{G}^D & \mathbf{G}^I & \mathbf{G}^C \end{pmatrix} \begin{pmatrix} \mathbf{q}^D \\ \mathbf{q}^I \\ \mathbf{q}^C \end{pmatrix}. \tag{25}$$

According to Eq. (24), $\mathbf{p}^I$ and $\mathbf{p}^D$ satisfy the relation:

$$\mathbf{P}^D = \mathrm{e}^{\mathrm{i}[\mathbf{ka}]_{xy}} \mathbf{P}^I, \tag{26}$$

for the normal derivatives $\mathbf{q}$, it has the opposite normal direction, so we have

$$\mathbf{q}^D = -\mathrm{e}^{\mathrm{i}[\mathbf{ka}]_{xy}} \mathbf{q}^I, \tag{27}$$

where $[\mathbf{ka}]_{xy} = k_x a_x$ when the relation between $\mathbf{P}^D$ and $\mathbf{P}^I$ is along the x direction, $[\mathbf{ka}]_{xy} = k_y a_y$ when the relation is along the y direction.

Substituting Eqs. (26) and (27) into Eq. (25), we obtain a system of equations represented only by the quantities of the independent and internal elements. Eq. (25) can be rewritten as follows:

$$\begin{pmatrix} \mathbf{B}^D \mathrm{e}^{\mathrm{i}[\mathbf{ka}]_{xy}} & \mathbf{B}^I & \mathbf{B}^C \end{pmatrix} \begin{pmatrix} \mathbf{p}^I \\ \mathbf{p}^I \\ \mathbf{p}^C \end{pmatrix} = \begin{pmatrix} -\mathbf{G}^D \mathrm{e}^{\mathrm{i}[\mathbf{ka}]_{xy}} & \mathbf{G}^I & \mathbf{G}^C \end{pmatrix} \begin{pmatrix} \mathbf{q}^I \\ \mathbf{q}^I \\ \mathbf{q}^C \end{pmatrix}. \tag{28}$$

Then, combining the coefficients column vectors corresponding to the same quantities, we obtain the following system of equations:

$$\begin{pmatrix} \mathbf{B}^D \mathrm{e}^{\mathrm{i}[\mathbf{ka}]_{xy}} + \mathbf{B}^I & \mathbf{B}^C \end{pmatrix} \begin{pmatrix} \mathbf{p}^I \\ \mathbf{p}^C \end{pmatrix} = \begin{pmatrix} -\mathbf{G}^D \mathrm{e}^{\mathrm{i}[\mathbf{ka}]_{xy}} + \mathbf{G}^I & \mathbf{G}^C \end{pmatrix} \begin{pmatrix} \mathbf{q}^I \\ \mathbf{q}^C \end{pmatrix}. \tag{29}$$

We finally obtain the following equations by moving the unknowns to the left-hand side,

$$\begin{pmatrix} \mathbf{B}^D \mathrm{e}^{\mathrm{i}[\mathbf{ka}]_{xy}} + \mathbf{B}^I & \mathbf{G}^D \mathrm{e}^{\mathrm{i}[\mathbf{ka}]_{xy}} - \mathbf{G}^I & \mathbf{A}^C \end{pmatrix} \begin{pmatrix} \mathbf{p}^I \\ \mathbf{q}^I \\ \mathbf{x}^C \end{pmatrix} = 0, \tag{30}$$

where $\mathbf{x}^C$ denotes the unknowns on the internal elements, and $\mathbf{A}^C$ denotes the coefficient matrix of $\mathbf{x}^C$. The constant elements guarantee that the number of dependent elements is equal to that of the independent elements, which results in a square system matrix. The Eq. (30) can be written in the form of a nonlinear Bloch's eigenvalue problem:

$$\mathbf{F}(\omega)(\mathbf{x}) = 0, \tag{31}$$

where $\mathbf{F}$ is a square matrix that contains ω implicitly and transcendentally. The highly nonlinear property makes it difficult to solve it by direct search method. In the next section, the block SS method is employed as a solver, which converts the nonlinear eigenvalue problem to a size-reduced linear eigenvalue problem.

2.4 The nonlinear Bloch eigenvalue problem solved by the block SS method

In order to solve the nonlinear Bloch eigenvalue problem given by Eq. (31), we use the block version of the SS method. The block SS method uses a set of arbitrary vectors rather than one. This technique raises the ability of obtaining more eigenvalues. For instance, let l be the number of the initial vectors and $2K-1$ be the maximun order of moment matrices, then $K \times l$ eigenvalues can be gained. This means that the solving procedure does not require a high-order moment matrix for calculating large number of eigenvalues. High order moment demands more interpolation points to keep accurate numerical results. However, every interpolation

point involves one BEM calculation, hence, low-order moment matrices are desirable to reduce the total computation time.

For the nonlinear Bloch eigenvalue problem given by Eq. (31), the m-order moment matrix is defined, as follows:

$$\mathbf{M}_m = \frac{1}{2\pi \mathrm{i}} \int_\Gamma \mathbf{U}^H \mathbf{F}(z)^{-1} \mathbf{V} z^m \mathrm{d}z, \qquad (m = 0, 1, 2, \cdots, K), \tag{32}$$

where Γ is a positive oriented Jordan curve in the complex plane of the wave number, $\mathbf{V}$ is formed by L nonzero arbitrary N dimensional column vectors, where N is the number of elements. $\mathbf{U}^H$ denotes the conjugate transpose of $\mathbf{U}$ and we choose as $\mathbf{U} = \mathbf{V}$ in this work.

The following generalized eigenvalue problem of two Hankel matrices, whose components consist of the above moment matrices, extracts the eigenvalues of the original nonlinear Bloch eigenvalue problem located within the contour integral path Γ,

$$\mathbf{H}_{Kl}^{<} \mathbf{w} = k \mathbf{H}_{Kl} \mathbf{w}, \tag{33}$$

where $\mathbf{H}_{Kl}^{<}$, $\mathbf{H}_{Kl}$ are written as, follows:

$$\mathbf{H}_{Kl} = \begin{pmatrix} \mathbf{M}_0 & \mathbf{M}_1 & \cdots & \mathbf{M}_{K-1} \\ \mathbf{M}_1 & \mathbf{M}_2 & \cdots & \mathbf{M}_K \\ \vdots & \vdots & \ddots & \vdots \\ \mathbf{M}_{K-1} & \mathbf{M}_K & \cdots & \mathbf{M}_{2K-2} \end{pmatrix}, \tag{34}$$

$$\mathbf{H}_{Kl}^{<} = \begin{pmatrix} \mathbf{M}_1 & \mathbf{M}_2 & \cdots & \mathbf{M}_K \\ \mathbf{M}_2 & \mathbf{M}_3 & \cdots & \mathbf{M}_{K+1} \\ \vdots & \vdots & \ddots & \vdots \\ \mathbf{M}_K & \mathbf{M}_{K+1} & \cdots & \mathbf{M}_{2K-1} \end{pmatrix}. \tag{35}$$

Further more, we transform the generalized eigenvalue problem to a standard linear eigenvalue problem. Since the number of eigenvalues is not known, the rank detection is carried out by using the singular value decomposition (SVD) as follows:

$$\mathbf{H}_{Kl} = \mathbf{C} \Sigma \mathbf{E}^H. \tag{36}$$

Let $\sigma_1, \sigma_2, \ldots, \sigma_{Kl}$ be the singular values of $\mathbf{H}_{Kl}$, the singular values corresponding to the eigenvalues actually existing in the integral path and the small singular values are separated by a threshold. The threshold is used to determine the rank of the Hankel matrices. Since the threshold values are not the same among different

problems, it is necessary to find the location of the gap in the singular values sorted in descendent order. We introduce another set of values $\delta_1, \delta_2, \ldots, \delta_{Kl-1}$:

$$\delta_{i-1} = \Delta\sigma_i = \frac{\log_{10}(\sigma_i) - \log_{10}(\sigma_{i-1})}{\Delta h}, \qquad (i = 2, 3, ..., Kl), \tag{37}$$

where $\Delta h = i - (i-1) = 1$. The set of δ_i implies the variation of singular values. If δ_i is larger than a threshold δ^*, it is indicated that the $(i+1)$-th singular value can be considered as a small singular value that should be removed. In this paper, we chose as $\delta^* = 1$. We note that Kl is rather small and the computation cost for SVD is negligibale.

Assuming that $i = m'$, where m' singular values are used for calculating the eigenvalues, an $m' \times m'$ matrix is obtained, as follows:

$$\mathbf{H}_{m'}\mathbf{y} = \lambda\mathbf{y}. \tag{38}$$

Let $\mathbf{H} = \mathbf{C}^H\mathbf{H}^{<}_{Kl}\mathbf{E}$, $\mathbf{H}' = \mathbf{H}(1:m', 1:m')$, and $\mathbf{H}_{m'} = {\Sigma_{m'}}^{-\frac{1}{2}}\mathbf{H}'\Sigma_{m'}^{-\frac{1}{2}}$, then the problem is converted to a linear eigenvalue problem of $\mathbf{H}_{m'}$, which can be solved by standard eigen-solver library directly.

The contour integration path is a circle since circular path retains a high accuracy for numerical calculation, and trapezoidal rule is employed to evaluate the contour integral.

3 Numerical examples

We give two examples to demonstrate the validity of the proposed method. The first one is a homogeneous problem: the cylinders are considered as rigid scatterers. The second example is a composite structure in which the cylindrical scatterers have a different material property, density, from that of the matrix medium. In the description of the second example, domain 1 (denoted by subscript '1') denotes the matrix medium and domain 2 (denoted by subscript '2') denotes the inclusions.

3.1 Homogeneous structure

We show in Fig. 4 the unit cell of the analysis model including rigid cylinders in the medium. The parameters of the homogeneous structure are shown in Tab. 1. The unit cell with the periodic boundary condition results in a plane exterior problem of a circular boundary.

We compute the eigenfrequencies of the structure with CBIE and Burton-Miller's method. The results are shown in Fig. 5 and Fig. 6, respectively. The integration

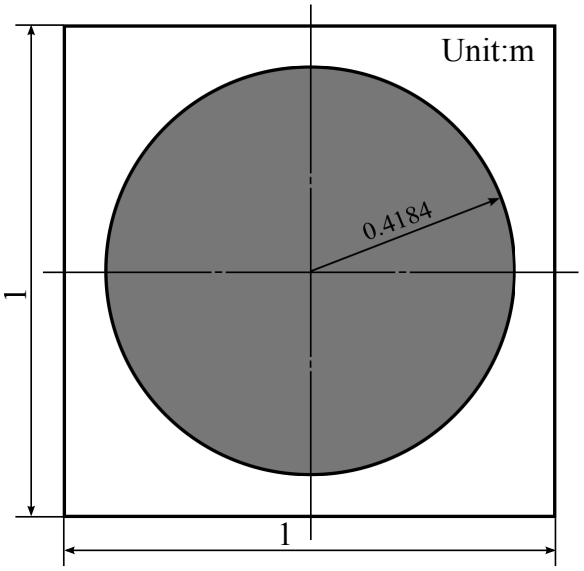

Figure 4: The unit cell with a rigid scatterer (the rigid scatterer is shown in gray and the matrix material is in white).

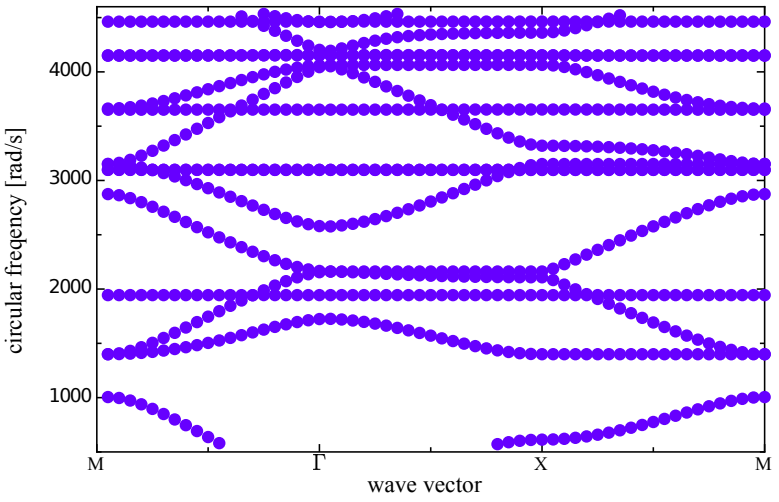

Figure 5: Dispersion curves obtained for the homogenous model by CBIE

Table 1: The parameters of homogenous structure

Domain	Density [kg/m^3]	Wave speed [m/s]	Filling fraction
1	$\rho_1 = 1.22$	$C_1 = 337.20$	$f = 0.55$

path is a circle in the complex plane, centered at $\gamma = (2550, 0)$ and its radius is $\rho = 2000$, the range of eigenvalues to calculate is $[550, 4550]$.

The dispersion curve in Fig. 5 indicates that some fictitious circular eigenfrequencies are also obtained, compared with previous research [Kushwaha (1997)]. When the wave vector k is varing, the fictitious eigenvalues are constants, observed as horizontal lines in Fig. 5. These real fictitious circular eigenfrequencies correspond to the boundary of the rigid cylinder with Neumann boundary condition. This means the eigenvalue problem for interior closed boundary is also computed by the block SS method.

These real fictitious circular frequencies satisfy

$$J_j\left(\frac{\omega R}{c}\right) = 0, \qquad (j = 0, 1, 2, \cdots), \tag{39}$$

where J_j is the Bessel function of the j-th order. The fictitious eigenfrequencies are related to the zeros of the Bessel function. These real fictitious eigenvalues are produced by the interior of the circular closed boundary, and they are called Neumann eigenvalues [Colton and Kress (1983)].

Since complex eigenvalues are also included in the results, we pick out the real ones by checking the values of the imaginary part. The imaginary part must satisfiy the following condition:

$$\frac{\mathrm{Im}(\omega)}{\rho} < \beta, \tag{40}$$

where β is a very small positive threshold. In the present work, it is taken as $\beta = 0.0085$.

However, those real fictitious circular frequencies cannot be distinguished in this way because they do not result from numerical error, but from a mathematical reason. Burton-Miller's method [Burton and Miller (1971)] can add a relatively large imaginary part to the real fictitious circular frequencies. Hence, we can exclude these fictitious frequencies from the results.

We find that from the comparisons of the results shown in Fig. 5 and Fig. 6 the horizontal lines formed by real fictitious circular frequencies are removed by applying

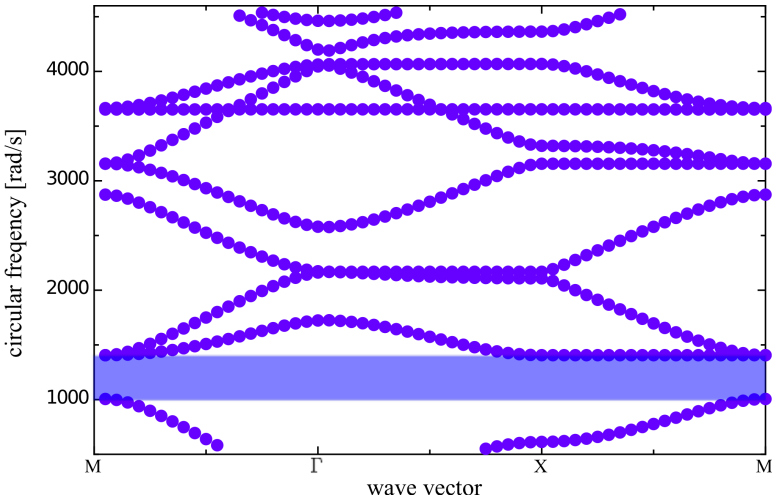

Figure 6: Dispersion curves obtained for the homogenous model by Burton-Miller's method. The shaded range implies the bandgap.

Burton-Miller's method. Actually, the real fictitious ones are moved to one side of the real axis, then eliminated by considering their large imaginary parts.

The dispersion curves illustrated in Fig. 6 show excellent agreement with the results given by the literature [Kushwaha (1997)].

3.2 Composite structure

We show in Fig. 7 a unit cell containing an inclusion in the medium. Tab. 2 contains the material constants and parameters of the composite structure. The structure of the previous example has a closed boundary, and Neumann boundary condition is given on it, however, the boundary of domain 1 of this example is the interface between domain 1 and domain 2.

Table 2: The parameters of composite structure

Domain	Density [kg/m^3]	Wave speed [m/s]	Filling fraction
1	$\rho_1 = 1.22$	$C_1 = 337.20$	$f = 0.5$
2	$\rho_2 = 0.09$	$C_2 = 1241.50$	

The results presented in this section are aimed to illustrate that the fictitious circular frequencies are also generated by the interior closed interface. It should be noted

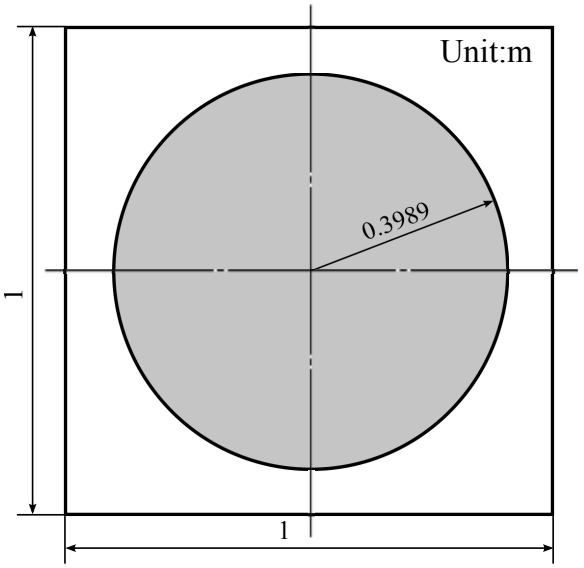

Figure 7: The nit cell with an inclusion (domain 2 is shown in gray and domain 1 is shown in white).

that the fictitious eigenfrequencies are decided by the material of domain 1 but not by that of domain 2. The results in Fig. 8 are also showing fictitious eigenfrequencies as those shown in Fig. 5. The boundary condition on the interior boundary between domain 1 and domain 2 is different from Neumann boundary condition in this example.

Because the filling fraction is different in this example, the real fictitious eigenfrequencies are different from those of the previous example, but, they also satisfy Eq. (39). This means that they are also the eigenfrequencies corresponding to the circular domain with the Neumann boundary condition on its boundary. It may be found in the results shown in Fig. 9 that the fictitious eigenfrequencies are also removed using Burton-Miller's method. For this phononic composite structure, we find two bandgaps in the band structure in the same range as that of Fig. 6.

4 Conclusion

The present approach has been demonstrated to be effective through the numerical examples for eigenfrequency analyses of periodic phononic structures. A methodology for calculations of band structures of acoustic phononic composite strucures is presented. This is achieved by combining the BEM with the block SS method.

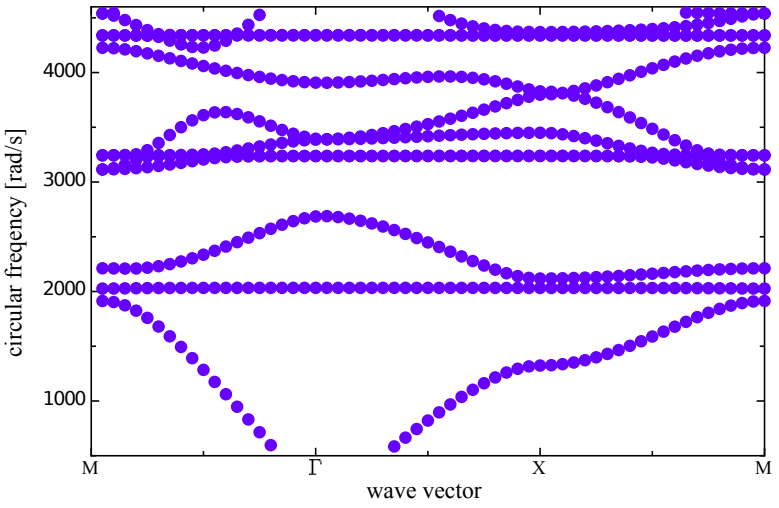

Figure 8: Dispersion curves of the composite model obtained by CBIE

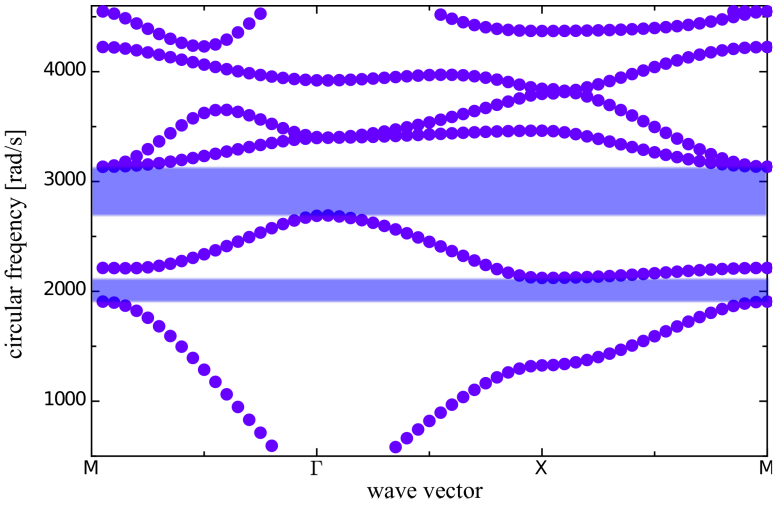

Figure 9: Dispersion curves of the composite model obtained by applying Burton-Miller's method. The shaded ranges imply the bandgaps.

The bandgaps have been observed correctly both in homogeneous and composite phononic structures. When applying the CBIE, the fictitious real eigenfrequencies have appeared in the dispersion curves as the eigenfrequencies of the inclusions with the Neumann boundary condtions. To exclude the fictitious eigenfrequencies, Burton-Miller's method, which adds a number that has a large imaginary component on the real fictitious ones, can be used.

Acknowledgement: The authors are grateful to the financial support to this work by JSPS KAKENHI Grant Number 23656121, and the China Scholarship Council (CSC) (File No. 2009612004)

References

Asakura, J.; Sakurai, T.; Tadano, H.; Ikegami, T.; Kimura, K. (2003): A numerical method for nonlinear eigenvalue problems using contour integrals. *JSIAM Lett.*, vol. 159, pp. 119–128.

Barnett, A.; Greengard, L. (2010): A new integral represntation for quasi-periodic fields and its application to two-dimensional band structure calculations. *J. Comput. Phys.*, vol. 229, pp. 6898–6914.

Burton, A. J.; Miller, G. F. (1971): The application of integral equation methods to the numerical solution of some exterior boundary-value problems. *Proc. Roy. Soc. Lond. A.*, vol. 323, pp. 201–210.

Colton, D.; Kress, R. (1983): *Integral Equation Methods in Scattering Theory*. John Wiley.

Gao, H. F.; Matsumoto, T.; Takahaishi, T.; Yamada, T. (2011): Eigenvalue analysis for 2D acoustic problem by BEM with block SS method. *Transactions of JASCOME*, vol. 11, pp. 107–110.

Goffaux, C.; Vigneron, J. P. (2001): Theoretical study of tunable phononic band gap system. *Phys. Rev. B*, vol. 64, 075118.

Ikegami, T.; Sakurai, T.; Nagashima, U. (2010): A filter diagnoalization for generalized eigenvalue problems based on the Sakurai-Sugiura projection method. *J. Comput. Appl. Math.*, vol. 233, pp. 1927–1936.

Kafesaki, M.; Economou, E. N. (1999): Multiple-scattering theory for three-dimensional periodic acoustic composites. *Phy. Rev. B*, vol. 60, 11993.

Khelif, A.; Choujaa, A.; Djafari-Rouhani, B.; Wilm, M.; Ballandras, S.; Laude, V. (2003): Traping and guiding of acoustic waves by defect modes in a full-band-gap ultrasonic crystal. *Phy. Rev. B*, vol. 68, 214301.

Khelif, A.; Djafari-Rouhani, B.; Vasseur, J. O.; Deymier, P. A. (2003): Transmission and dispersion relations of perfect and defect-containing waveguide structures in phononic band gap materials. *Phy. Rev. B*, vol. 68, 024302.

Knipp, P. A.; Reinecke, T. L. (1998): Boundary-element calculations of electromagnetic band-structure of photonic crystals. *Physica. E*, vol. 2, pp. 920–924.

Kushwaha, M. S. (1997): Stop-bands for periodic metallic rods: Sculptures that can fillter the noise. *Appl. Phys. Lett.*, vol. 70, pp. 3218–3220.

Kushwaha, M. S.; Halevi, P.; Dobrzynski, L.; Djafari-Rouhani, B. (1993): Acoustic band structure of periodic elastic composite. *Phy. Rev. Lett.*, vol. 71, pp. 2022–2025.

Li, F. L.; Wang, Y. S.; Zhang, C. Z. (2012): Boundary element method for bandgap computation of photonic crystals. *Opt. Commun.*, vol. 285, pp. 527–532.

Liu, Z. Y.; Chan, C. T.; Sheng, P. (2002): Three-component elastic wave band-gap material. *Phy. Rev. B*, vol. 65, 165116.

Martínez-Sala, R.; Sancho, J.; Sánchez, J. V.; Gómez, V.; Llinares, J. (1995): Sound attenuation by sculpture. *Nature*, vol. 378, pp. 241.

Parmley, S.; Zobrist, T.; Clough, T.; Perez-Miller, A.; Makela, M.; Yu, R. (1995): Phononic band structure in a mass chain. *Appl. Phys. Lett.*, vol. 67,777.

Psarobas, I. E.; Stefanou, N.; Modinos, A. (2000): Scattering of elastic waves by periodic array of spherical bodies. *Phy. Rev. B*, vol. 62, 278.

Qian, Z. Y.; Han, Z. D.; Atluri, S. N. (2004): Directly Derived Non-Hyper-Singular Boundary Integral Equation for Acoustic problems, and Their Solution through Petrov-Galerkin Schemes. *CMES: Computer Modeling in Engineering & Sciences*, vol. 5, no. 6, pp. 541–562.

Qian, Z. Y.; Han, Z. D.; Ufimtsev, P.; Atluri, S. N. (2004): Non-Hyper-Singular Boundary Integral Equations for Acoustic Problems, Implemented by the Collocation-Based Boundary Element Method. *CMES: Computer Modeling in Engineering & Sciences*, vol. 6, no. 2, pp. 133–144.

Sakurai, T.; Kodaki, Y.; Tadano, H.; Takahashi, D.; Sato, M.; Nagashima, U. (2008): A parallel method for large sparse generalized eigenvalue problems using a GridRPC system. *Future Gener. Comput. Syst.*, vol. 24, pp. 613–619.

Sakurai, T.; Sugiura, H. (2003): A projection method for generalized eigenvalue problems using numerical integration. *J. Comput. Appl. Math.*, vol. 159, pp. 119–128.

Sigalas, M.; Economou, E. N. (1993): Band structure of elastic waves in two dimensional systems. *Solid State Commun*, vol. 86, pp. 141–143.

Sigalas, M. M. (1998): Defect states of acoustic waves in a two-dimensional lattice of solid cylinders. *J. Appl. Phys.*, vol. 84, 3026.

Tanaka, Y.; Tomoyasu, Y.; Tamura, S. (2000): Band structure of acoustic waves in phononic lattice: two-dimensional composites with large acoustic mismatch. *Phy. Rev. B*, vol. 62, 7387.

Tsuchimochi, T.; Kobayashi, M.; Nakata, A.; Imamura, Y.; Nakai, H. (2008): Application of the Sakuarai-Sugiura Projection Method to Core-Excited-State Calculation by Time-Dependent Density Functional Theory. *J. Comput. Chem.*, vol. 29, pp. 2311–2316.

Vasseur, J. O.; Deymier, P. A.; Khelif, A.; Lambin, P.; Djafari-Rouhani, B.; Akjouj, A.; Dobrzynski, L.; Fettouhi, N.; Zemmouri, J. (2002): Phononic crystal with low filling fraction and absolute acoustic band gap in the audible frequency range: A theoretical and experimental study. *Phy. Rev. E*, vol. 65, 056608.

Wang, W.; Wen, J. H.; Han, X. Y.; Zhao, H. G. (2003): Finite difference time domain method for the study of band gap in two-dimensional phononic crystals. *Acta Phy. Sin. -Ch. ed.*, vol. 52, pp. 1943–1947.

Yan, Z. Z.; Wang, Y. S. (2006): Wavelet-based method for calculating elastic band gaps of two-dimensional phononic crystals. *J. Comput. Phys*, vol. 74, 224303.

Zheng, C. J.; Chen, H. B.; Matsumoto, T.; Takahashi, T. (2011): Three dimensional acoustic shape sensitivity analysis by means of adjoint variable method and fast multipole boundary element approach. *CMES: Computer Modeling in Engineering & Sciences*, vol. 79, pp. 1–29.